Analysis and Modeling of Mid-Latitude Decameter-Scale Plasma Wave Irregularities Utilizing GPS and Radar Observations

A. Eltrass[1], W. A. Scales[1], P. J. Erickson[2], J. M. Ruohoniemi[1], J. B. H. Baker[1]

[1] Bradley Department of Electrical and Computer Engineering, Virginia Tech, Blacksburg, Virginia, USA.

[2] MIT Haystack Observatory, Massachusetts Institute of Technology, Westford, Massachusetts, USA.

Abstract

The mid-latitude SuperDARN radars frequently observe decameter-scale irregularities in the nightside sub-auroral ionosphere during quiet and active geomagnetic periods, however, the mechanism responsible for the growth of such irregularities has not yet been established. In this paper, the Temperature Gradient Instability (TGI) and the Gradient Drift Instability (GDI) are extended into the kinetic regime appropriate for HF radar frequencies and analyzed as the cause of these irregularities. Based on the coordination between the Millstone Hill Incoherent Scatter Radar (ISR) and the Blackstone SuperDARN radar, a time series for the growth rate of both TGI and GDI is calculated for observations in the sub-auroral ionosphere under quiet and disturbed geomagnetic conditions. The potential impact of the mid-latitude ionospheric irregularities on GPS signals is investigated utilizing modeling and observations. The recorded GPS scintillation data are analyzed to monitor the amplitude scintillations and to obtain the spectral characteristics of irregularities producing ionospheric scintillations. The nonlinear evolution of the mid-latitude ionospheric TGI is studied utilizing gyro-kinetic Particle-In-Cell (PIC) simulation techniques with Monte Carlo collisions, allowing further investigation of the TGI as the cause for the SuperDARN observations. The spatial power spectra of the density fluctuations associated with the TGI are calculated and compared with both GPS spectral results and previous in-situ satellite spectral measurements. The spectral calculations suggest that initially TGI or/and GDI irregularities are generated at large scale size or sizes (km-scale) and the dissipation of the energy associated with these irregularities occurs by generating smaller and smaller (decameter-scale) irregularities. The reasonable agreement between experimental, theoretical, and computational results of this study suggests that a TGI turbulent cascade may be responsible for the observed quiet-time decameter-scale irregularities, while turbulent cascade processes of TGI and GDI may cause the mid-latitude ionospheric irregularities that result in GPS scintillations during disturbed-times. The results also reveal that the E-region may be responsible for shorting out the F-region TGI and GDI electric fields before and around sunset and ultimately leading to irregularity suppression.

1. Introduction

Ionospheric irregularities are small-scale structures in the plasma density created by various plasma instabilities, which are driven by combinations of plasma drifts, density and temperature gradients, and electric fields [e.g., Fejer and Kelley, 1980]. The scale sizes of these irregularities range from thousands of kilometers down to a few centimeters. Recent works indicate that the mid-latitude ionosphere is more active than currently appreciated, and that ionospheric processes producing the mid-latitude GPS scintillations are less understood due to lack of models and observations that can explain their characteristics and distributions [e.g., Kelley, 2009]. During geomagnetically quiet conditions ($K_p \leq 2$), the mid-latitude ionosphere (30° to 60° geomagnetic latitude) is a quiescent plasma but still populated by plasma density irregularities generated by both plasma and neutral processes.

The mid-latitude decameter-scale ionospheric irregularities with scale lengths on the order of 10 m were studied early through the detection of backscatter echoes observed by High-Frequency (HF) radars [e.g., Oksman et al., 1979]. The Super Dual Auroral Radar Network (SuperDARN) consists of chains of HF radars that cover middle- and high-latitudes in both hemispheres. SuperDARN radars monitor the ionospheric dynamics through the detection of decameter-scale ionospheric plasma irregularities in the E- and F-regions [e.g., Chisham et al., 2007]. The mid-latitude SuperDARN radars revealed decameter-scale ionospheric irregularities during quiet geomagnetic periods that have been proposed to be responsible for the observed low-velocity Sub-Auroral Ionospheric Scatter (SAIS) [e.g., Greenwald et al., 2006]. Despite their high occurrence rate and large geographical spread, the plasma instability mechanism responsible for the growth of these irregularities is still unknown. A quantitative analysis of growth rates and time-scales of feasible plasma instabilities is required to identify what mechanisms predominate.

The storm-time ionospheric irregularities at mid-latitudes are sufficiently strong to cause signal power fluctuations, known as ionospheric scintillation, in transionospheric satellite transmissions such as the Global Position System (GPS) [e.g., Basu et al., 2001; Ledvina et al., 2002]. This raises the importance of knowing the cause and distribution of these ionospheric plasma irregularities to maintain the performance of satellite-ground data transmission. Basu et al. [2001] and Ledvina et al. [2002] reported intense mid-latitude UHF and L1-band scintillations within structured Sub-Auroral Plasma Streams (SAPS) over the eastern continental United States. Using satellite data from the Defense Meteorological Satellite Program (DMSP), Mishin et al. [2003] determined that small-scale density, electric field, velocity, and electron temperature structures can occur in SAPS storm-time mid-latitude trough structures. Keskinen et al. [2004] suggested that the TGI in association with the GDI could be responsible for generating these small-scale structures in the trough wall region. Although the TGI and GDI are suggested to be responsible for the observed mid-latitude irregularities, more detail is not known about the exact role of these plasma instabilities in generating the sub-auroral irregularities [e.g., Kelley, 2009]. Important effects to be considered in further detail include different spatial scales, nonlinear cascading, and the impact of E-region conductance.

The aim of this work is to model and analyze the observed decameter-scale ionospheric plasma wave irregularities at mid-latitudes through the coordination between the Blackstone SuperDARN radar, the Millstone Hill ISR, and GPS receivers under various sets of geomagnetic conditions. In section 2, the linear kinetic theory of TGI and GDI is presented to provide perspective on the experimental observations. Section 3 illustrates the co-located experimental observations by the Blackstone SuperDARN radar, and the Millstone Hill ISR. Next, a critical comparison of TGI and GDI is made by the calculation of TGI and GDI growth rate time series for these observations. Section 4 discusses the nonlinear gyro-kinetic simulation of the ionospheric TGI over a broad set of parameter regimes. In section 5, the GPS scintillation data are analyzed to monitor the amplitude scintillations and to obtain the spectral characteristics of irregularities producing ionospheric scintillations at mid-latitudes. Next, the GPS spectral measurements on the ground are calculated and compared with both simulation results and previous in-situ satellite spectral measurements. In section 6, the conclusion is provided.

2. Theory

The TGI derives its free energy from the opposed temperature and density gradients in the F-region in the plane perpendicular to the magnetic field [Hudson and Kelley, 1976]. If perturbations to a boundary between hotter and cooler plasma regions occur, the electrons will convect and generate charge accumulation at the interface causing the formation of a polarization electrostatic field E in the presence of the ambient magnetic field B [e.g., Eltrass and Scales, 2014]. These polarization fields grow as a consequence of the diamagnetic drifts of the opposed density and temperature gradients, and thus enhance the perturbation. In contrast, when the electron density and temperature gradients are aligned, the diamagnetic drifts will be such that the magnitude of the polarization field will be decreased and the magnitude of the perturbation will decay due to the resonance electron interactions with the TGI waves. The TGI kinetic electrostatic dispersion relation has been solved with full kinetic effects for Landau damping, finite gyro-radius $k_{\perp}\rho_{ci} \geq 1$, temperature anisotropy, and electron collisions [Eltrass et al., 2014]. The TGI wave frequency and growth rate are calculated at 300 km altitude in a region of opposed temperature and density gradients relevant to SuperDARN observations.

The GDI is an interchange instability process that is known to cause irregularities in the F-region ionosphere. This instability can occur in an inhomogeneous, weakly collisional, magnetized plasma that contains an ambient electric field orthogonal to both the magnetic field B and the density gradient κ_n. Despite a good level of theoretical understanding of large-scale GDI irregularities, more studies are required at small spatial scales [Kelley, 2009]. The observations discussed in this study examine wavelengths of around 10-15 m, which is where kinetic effects begin to play a role and the kinetic theory must be employed. Therefore, the GDI kinetic dispersion relation based on the Gary and Cole [1983] model is used here to allow the study of GDI for short wavelengths (decameter-scale waves of SuperDARN observations).

3. Experimental Radar Observations

During the nights of 15-16 October 2014 (quiet geomagnetic conditions $K_p \leq 2$) and 10-11 October 2014 (active geomagnetic conditions $3 < K_p \leq 4$), the Blackstone SuperDARN radar (37.10° N, 282.05° E) and the Millstone Hill ISR (42.6° N, 288.5° E) were running co-located observations of sub-auroral ionospheric irregularities. Figure 1 shows the backscatter power in dB and the line-of-sight Doppler velocity in m/s along beam 13 for both experiments. The observations during the two events show both types of backscatter, ground and ionospheric scatter. First, the scatter from higher magnetic latitudes over the time interval 00:00 to 02:00 UT is ground

backscatter. After 02:00, the radar begins to observe ionospheric scatter with a small Doppler velocity during the quiet-time experiment and a relatively large Doppler velocity during the active time experiment over latitudes from 54° to 60° on most of the radar beams. The ionospheric irregularities responsible for the observed scatter are seen in the top-side F-region ionosphere and extend uniformly across the radar field-of-view.

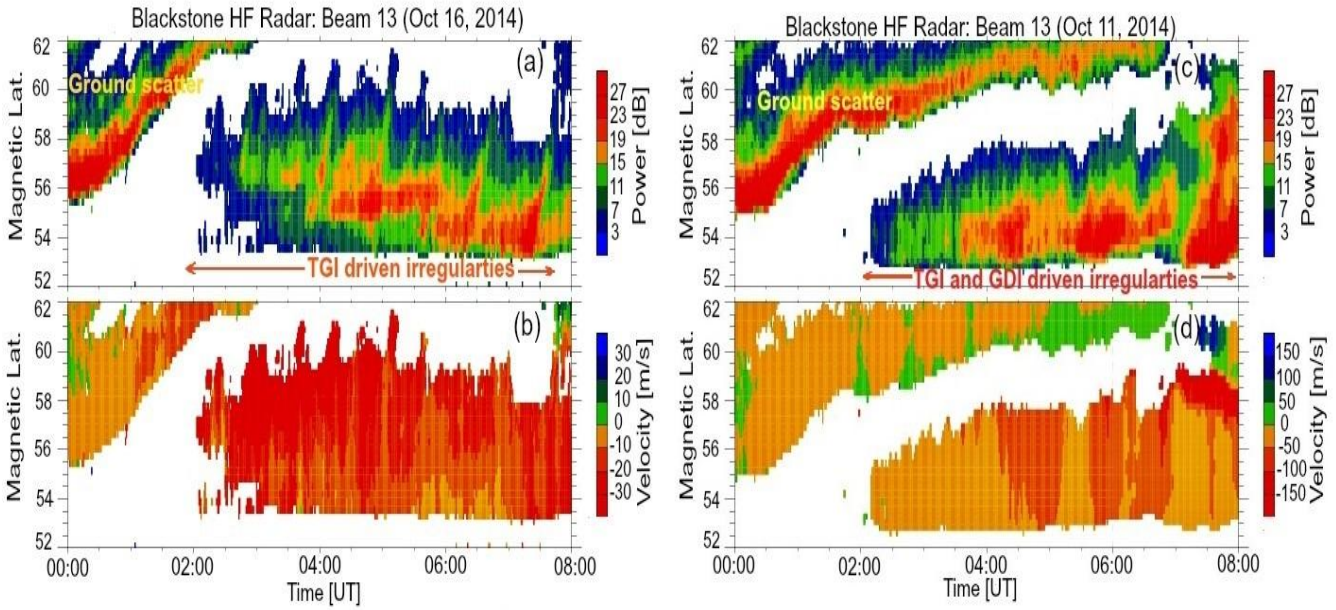

Figure 1: Backscatter echoes from the Blackstone SuperDARN radar on the nights of October 15-16 and October 10-11, 2014. Backscatter power and line-of-sight Doppler velocity measured along beam 13 during the two events are shown in panels (a, c) and (b, d), respectively.

In order to determine the physical mechanisms responsible for the observed ionospheric irregularities, the data from the Millstone Hill ISR are used. The geometry used in the investigation of the TGI and GDI at the mid-latitude ionosphere is shown in Figure 2. Combining measurements from the zenith and azimuth scans, the horizontal and vertical gradients are calculated. Within the region of interest to this study, the geomagnetic field lines are inclined at about 70°. Note that none of the Millstone Hill ISR pointing directions are perpendicular to the geomagnetic field B, while the gradients required in the TGI and GDI theories are those perpendicular to B [e.g., Eltrass et al., 2014; Gary and Cole, 1983]. The density and temperature gradients are calculated in the direction perpendicular to B in the top-side F-region by first estimating the vertical gradients with a linear least square fit along the zenith direction, and then adding their projection onto the direction perpendicular to B to the projection of the horizontal gradients onto the same direction (see Figure 2).

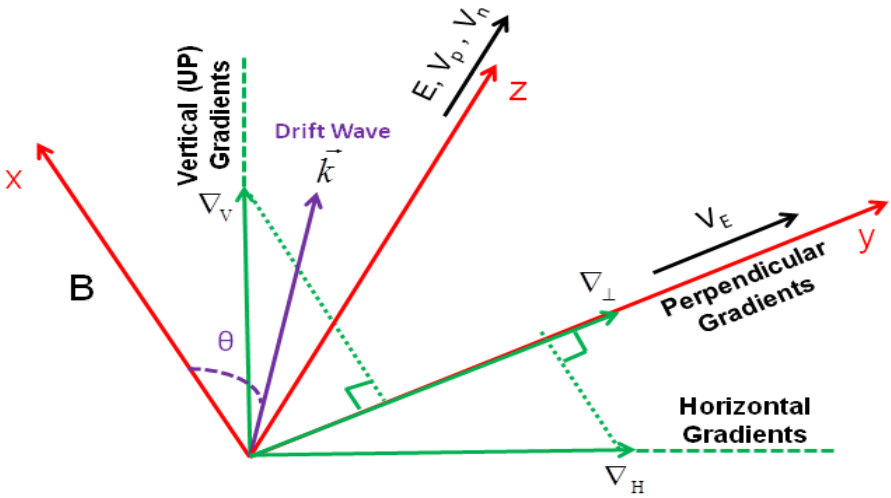

Figure 2: The TGI and GDI geometry in the mid-latitude ionosphere relative to the Earth's magnetic field, the temperature and density gradient, diamagnetic and Pedersen drifts, and the wave vector of resistive drift waves. The perpendicular temperature and density gradients are calculated as the sum of the projections of the horizontal and vertical gradients.

A critical comparison of TGI and GDI is made for the mid-latitude SuperDARN observations at the nightside by the development of the growth rate time series of both TGI and GDI. Figures 3a and 3b show the TGI and GDI growth rates for quiet- and disturbed-time events, respectively. Figure 3a shows that the TGI exceeds the GDI growth rate by a factor of 9-10 and dominates for the duration of the quiet-time experiment, explaining the observed low-velocity SAIS between 02:00 and 08:00 UT shown in Figure 1b. This suggests that the observed decameter-scale ionospheric irregularities under quiet conditions are produced by the TGI or a cascade product from it, while the GDI does not have a significant role in the generation of these irregularities. On the other hand, Figure 3b shows the large growth for both TGI and GDI during the disturbed-time experiment, suggesting that the TGI in concert with the GDI may cause the observations of disturbed-time mid-latitude ionospheric irregularities shown in Figure 1c. Comparing Figures 3a and 3b, the TGI and GDI growth rates during the disturbed-time event are larger than those of the quiet-time event. This is because the disturbed F-region is characterized by smaller scale lengths, larger electric fields, and larger temperature ratios (T_e / T_i), which would imply larger growth rate [Eltrass et al., 2014]. At the beginning of both experiments, the TGI and GDI growth rates may not be observed by the Blackstone radar due to signal propagation effects in which the radar signals encounter these irregularities under unsuitable magnetic aspect conditions or do not encounter them at all [e.g., Davies, 1990]. Another reason for the delay between sunset and irregularity observations could be the E-region as the controlling factor for irregularity growth.

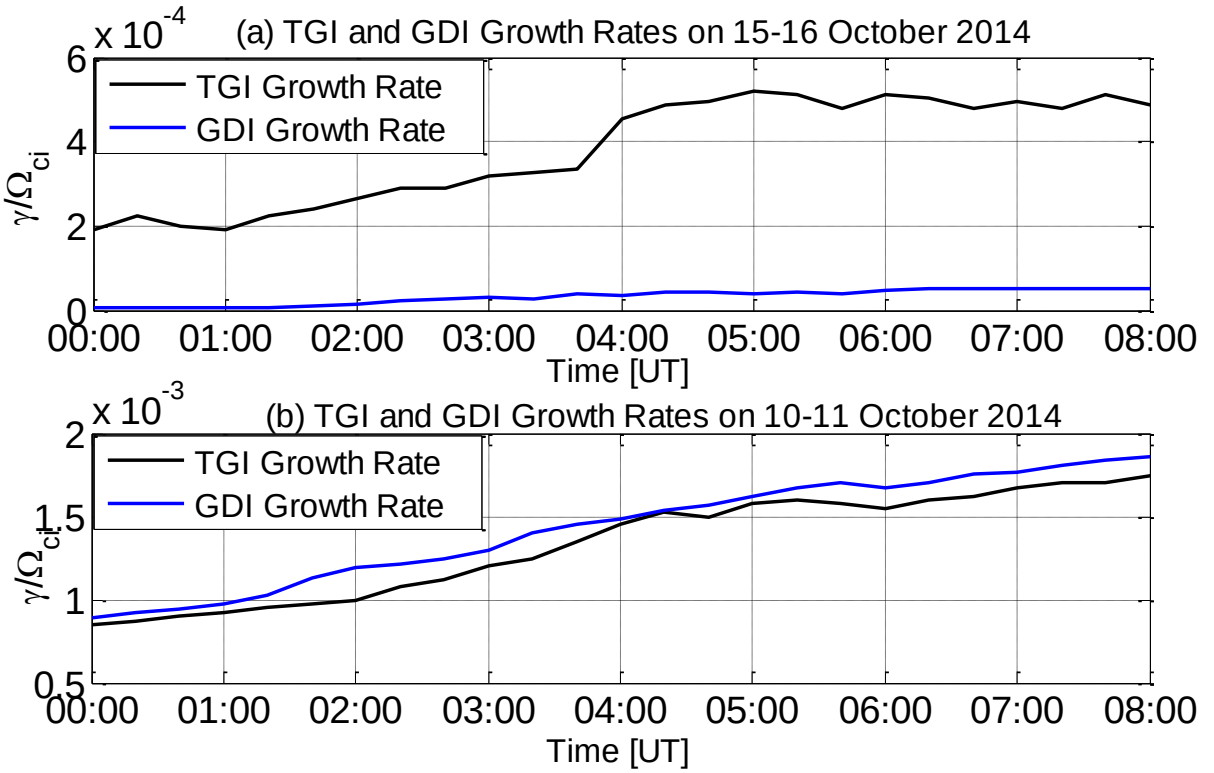

Figure 3: The time series of TGI and GDI growth rates on the nights of (a) October 15-16 and (b) October 10-11, 2014. The growth rates are calculated over the wavelength range $1 < k\rho_{ci} < 1.5$, which corresponds to the operating frequency range of the Blackstone SuperDARN radar throughout the two experiments.

4. Gyro-Kinetic Simulation Model and Results

Although the linear theory of section 2 provides the insight for the initial TGI growth, it cannot fully describe the nonlinearly saturated behavior as observed by radars. In order to investigate such nonlinear effects, e.g., wave cascading, the gyro-kinetic simulation model [e.g., Eltrass and Scales, 2014], which contains the nonlinearities relevant to F-region irregularities, is employed. A periodic two-dimensional Particle-In-Cell (PIC) electrostatic computational model is utilized to investigate the nonlinear evolution of the TGI in the mid-latitude ionosphere. The dominant ion species at the altitude 300 km relevant to SuperDARN observations is O^+, which implies the use of $m_i / m_e = 16 \times 1836$. The simulation parameters of the current scheme in units of grid size Δ and ion cyclotron frequency Ω_{ci} are $L_x \times L_y = 256\Delta \times 512\Delta$ with cell sizes $\Delta x = \Delta y = 2.67$ m, N (total number of

simulation particles per species) $= 49\times256\times512$, $\rho_{ci} = \Delta = 1$, $T_e / T_i = 1$, $\kappa_n \rho_{ci} = 1\times10^{-3}$, $\kappa_T \rho_{ci} = 2\times10^{-3}$, time step $= \Omega_{ci}\Delta t = 2.5$, and the number of time steps is 1400.

In order to provide the most important physics of the TGI evolution, three TGI simulations, with normalized electron collision frequency of $\upsilon_e / \Omega_{ce} = 0.0, 3.4\times10^{-5}$, and 9.1×10^{-5}, were performed. Figure 4a shows that the TGI instability exhibits two distinct stages of development, i.e., the linear growth stage that fits the predictions of linear theory in section 2 and the subsequent nonlinear evolution associated with saturation. The normalized field energy for the three simulations are shown in Figure 4a. With the introduction of collisions, the TGI instability grows faster and the saturation amplitude is greatly enhanced by collisions and appears to be rapidly approaching an upper bound $q\Phi / k_B T_e \approx (\omega / \Omega_{ci}) / (k_\perp \rho_{ci})^2$ as a function of $\sqrt{\upsilon_e}$ [Eltrass and Scales, 2014]. The linear growth rates of the three runs are in reasonable agreement with the maximum growth rates for their respective values of υ_e using the linear theory.

Focusing on the third run $\upsilon_e / \Omega_{ce} = 9.1\times10^{-5}$, which corresponds to unscaled υ_e = 800 Hz of ionospheric altitude 300 km, the spatial power spectra $P(k_y)$ of the density fluctuations associated with the TGI instability are computed, where k_y is the dominant direction of propagation of the drift waves. The density perturbations can be represented by power-laws k^{-n}, where n is the irregularity spectral index. Figure 4b illustrates the 1-D power spectral densities as a function of spatial wave number. The density spatial power spectra are well presented by a power-law $P(k_y) \propto k_y^{-n_y}$, with the spectral index $n_y = 2.2 \pm 0.2$. The spectra calculations of TGI density irregularities lie in the same range of previous numerical simulations of the GDI [e.g., Keskinen, 1984; Keskinen and Huba, 1990], showing that the spectral index of TGI and GDI density irregularities are of the order 2. This suggests that a turbulent cascade process occurs from km-scale (linear growth stage) to the decameter-scale irregularities (saturation stage) as would be observed by the SuperDARN radars.

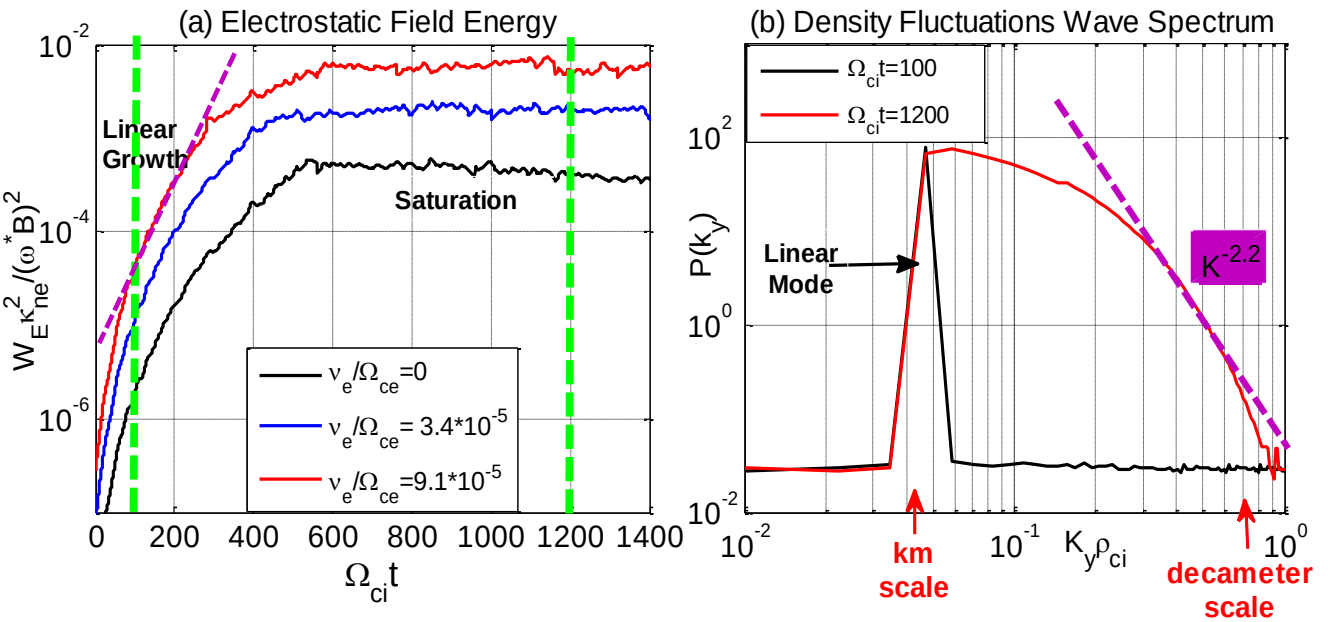

Figure 4: (a) Normalized electrostatic field energy for TGI simulations with varying electron collision frequency. (b) The time evolution of the 1-D electron density wave number spectrum for the third run $\upsilon_e / \Omega_{ce} = 9.1\times10^{-5}$, which is most applicable for SuperDARN observations at altitude 300 km. The spectral index *n* =2.2 is calculated from the linear slope of electron density spectrum.

5. GPS Measurements

Ionospheric scintillation measurement is recorded using Connected Autonomous Space Environment Sensor (CASES) GPS receivers at Virginia Tech University (37.205° latitude, -80.417° longitude, and 620.33 m altitude). The recorded GPS data are analyzed to monitor the amplitude scintillations at mid-latitudes under

various sets of geomagnetic and seasonal conditions. The amplitude scintillation index S_4 is used to estimate the intensity of the observed scintillation. The S_4 index is defined as the ratio of the standard deviation of the received signal power to the average signal power computed over a period of time [Briggs and Parkin, 1963]. The S_4 index is normally detrended by separating scintillation from thermal noise, multi-path, and other impacts [Van Dierendonck et al., 1993]. In this work, we have taken the value of S_4 index 0.2 as the threshold value of the ionospheric amplitude scintillation. During the night of 10-11 October ($3 < K_p \leq 4$), S_4 indices reached a peak value of approximately 0.35, indicating a scintillation activity. For some nights with K_p = 5 or more, S_4 indices reached values up to 0.6, revealing a strong scintillation activity. Such events can degrade or even disrupt communication and navigation systems relying upon transionospheric radio wave propagation.

The scintillation measurements are also analyzed to obtain the spectral characteristics of irregularities producing ionospheric scintillations at mid-latitudes. The power spectrum of a scintillation event is calculated for every 5 minutes of data interval (3000 data points) via Fast Fourier Transform (FFT) to obtain the spectral index of the density irregularities (p). Figure 5a shows the power spectra of amplitude scintillation at 04:50 UT on October 11, 2014 computed for the raw data to get the GPS spectral index. As shown in Figure 5a, there are three main portions of scintillation power spectra: low frequency portion in the left, then the high frequency roll-off part which contains the information about the ionospheric irregularities, and finally the noise floor in the right. The Fresnel frequency can be defined as the transition frequency between the low frequency and the high frequency roll-off part. Since the scintillations discussed in this work are weak to moderate, the spectrum of received signal follows a power-law spectrum with a single slope [e.g., Singleton, 1974]. Consequently, the spectral slope (p) is estimated from the linear high frequency roll-off portion of the log-log plot of power spectrum by fitting a straight line to the steepest part using the least square technique [e.g., Banola et al., 2005]. As shown in Figure 5a, the power spectral index for the irregularities is calculated and found to be 2.8. Note that the power falls off as f^{-p} for frequencies f above the roll-off frequency when the ionospheric irregularities follow a power-law k^{-n}, where k is the irregularity wave vector. The in-situ irregularity spectral index n can be related to the ground spectral index p by $n = p - 1$ [e.g., Bhattacharyya and Rastogi, 1985, 1991]. The GPS spectral indices are slightly different than those in the irregularity spectra ($n = p - 1$) because of the nonlinear transformations on the signal propagating through the irregularity and space.

Figure 5b shows the relationship between the S_4 index and the spectral index p for scintillation measurements during January-December 2014. The spectral index for the data under consideration ranges from 2.2 to 2.8. The results indicate that the spectral index increases with S_4 indices for weak to moderate scintillation ($0.1 < S_4 \leq 0.4$). However, for strong scintillation ($S_4 > 0.4$), the spectral index seems to be a constant value. The average value of the GPS spectral index is $p = 2.5$, which is comparable to the mid-latitude measured in-situ irregularity spectral index minus one [e.g., Foster and Rich, 1998; Mishin and Blaunstein, 2008].

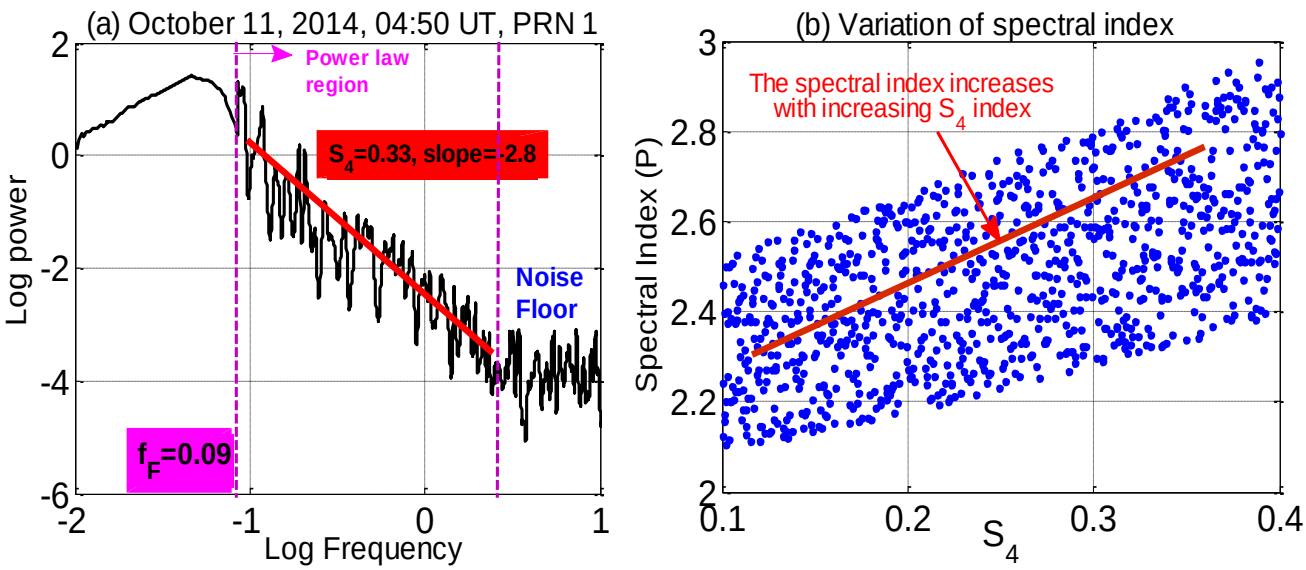

Figure 5: (a) Power spectra of amplitude scintillation recorded at 04:50 UT on October 11, 2014. The spectral index p and the Fresnel frequency f_F are 2.8 and 0.09 Hz, respectively. The selected portion for estimating the spectral index is shown by two vertical dashed lines. (b) Variation of spectral index (p) with amplitude scintillation index (S_4) for scintillation measurements during January-December 2014.

Using DMSP satellite data, Mishin and Blaunstein [2008] calculated the power spectral densities of mid-latitude irregularities as a function of spatial wave number during scintillation intervals on 26 September 2001. They showed that the power spectra of the density irregularities corresponding to spatial wavelengths between several hundred meters and several tens of meters admit a power-law characterization k^{-n} with a spectral index $1.7 < n < 2$. The data available to this study are not sufficient to use in-situ satellite measurements and calculate the power spectral densities for the events under investigation. However, the spectra simulations of TGI and GDI density irregularities [e.g., Eltrass and Scales, 2014; Keskinen, 1984] along with ground GPS measurements are in reasonable agreement with DMSP satellite measurements for previous disturbed-time events in the nightside sub-auroral ionosphere [e.g., Foster and Rich, 1998; Mishin et al., 2003; Mishin and Blaunstein, 2008]. Also, the growth times for the disturbed mid-latitude irregularities are on the order of several minutes [e.g., Mishin and Blaunstein, 2008; Keskinen et al., 2004], which is consistent with the TGI and GDI simulation results. An interpretation of the spectral analysis is that TGI and GDI irregularities are initially generated at kilometer-scale, become unstable and dissipate their energy by generating smaller sized (decameter-scale) irregularities. This suggests that decameter- and large-scale irregularities may co-exist under disturbed conditions of the mid-latitude F-region ionosphere. Note that ionospheric structures on the order of the Fresnel radius (i.e., 350-400 m for L-band) will contribute mostly to the observed scintillations, while irregularities of smaller-scales will introduce less amplitude fluctuations.

6. Conclusion

This work has investigated the TGI and GDI as the cause of mid-latitude decameter-scale ionospheric irregularities observed by the SuperDARN radars during quiescent and disturbed geomagnetic conditions. The TGI and GDI are accessed as the cause of these irregularities by developing kinetic models that extend into the kinetic regime, include finite ion gyro-radius effects, and underscore limitations in fluid theory for short wavelengths. Co-located experimental observations by the Blackstone SuperDARN radar, and the Millstone Hill ISR are performed under quiet and disturbed sets of geomagnetic conditions to identify what plasma instability mechanisms predominate. A time series for the growth rate of both TGI and GDI is developed for these events, showing that the TGI is the most likely generation mechanism for quiet-time irregularities, while the TGI in association with the GDI may be responsible for the disturbed-time observations. The nonlinear evolution of the mid-latitude ionospheric TGI is investigated utilizing gyro-kinetic PIC simulation techniques with Monte Carlo collisions. The simulation results show important consequences of nonlinear evolution, particularly wave cascading of TGI from kilometer-scales into the decameter-scale regime of the radar observations. The GPS measurements show scintillations of GPS L1 signals occurring at mid-latitudes in the presence of ionospheric irregularities during disturbed geomagnetic conditions. The GPS spectral indices of the spectra observed on the ground are computed and found to be consistent with both TGI and GDI numerical simulations and previous in-situ satellite measurements during disturbed periods [e.g., Mishin and Blaunstein, 2008]. This shows that the spectral index of mid-latitude density irregularities with scale sizes less than 1 km are of the order 2. The scintillation results along with radar observations suggest that the observed decameter-scale irregularities that cause SuperDARN backscatter, co-exist with kilometer-scale irregularities that cause L-band scintillations. The alignment between the experimental, theoretical, and computational results of this study suggests that turbulent cascade processes of both TGI and GDI may cause the observations of mid-latitude GPS scintillations during disturbed geomagnetic conditions. This also lends further support to the belief that the absence of the observed irregularities before and around sunset is due to the high E-region conductivity, which leads to the suppression of irregularity growth. Further insight requires the coordination between in-situ satellite measurements, ground radar observations, and GPS data at mid-latitudes under various sets of geomagnetic and seasonal conditions.

7. References

1. Banola, S., B. M. Pathan, D. R. K. Rao, and H. Chandra (2005), Spectral characteristics of scintillations producing ionospheric irregularities in the Indian region, *Earth Planets Space*, 57, 47-59.
2. Basu, S., C. E. Valladares, H. C. Yeh, S. Y. Su, E. MacKenzie, P. J. Sultan, J. Aarons, F. J. Rich, P. Doherty, K. M. Groves, and T. W. Bullett (2001), Ionospheric effects of major magnetic storms during the International Space Weather Period of September and October 1999: GPS observations, VHF/UHF scintillations, and in situ density structures at middle and equatorial latitudes, *J. Geophys. Res.*, 106, 30, 389.
3. Bhattacharyya, A., and R. G. Rastogi (1985), Amplitude scintillation during early and late phases of evolution of irregularities in the nighttime equatorial ionosphere, *Radio Sci.*, 20(4), 935-946.
4. Bhattacharyya, A., and R. G. Rastogi (1991), Structure of ionospheric irregularities from amplitude and phase scintillation observations, *Radio Sci.*, 26(2), 439-449.
5. Briggs, B. H., and I. A. Parkin (1963), On the variation of radio star and satellite scintillation with zenith angle, *J. Atmos. Terr. Phys.*, 25, 339-365.

6. Chisham, G., M. Lester, S. E. Milan, M. P. Freeman, W. A. Bristow, A. Grocott, K. A. McWilliams, J. M. Ruohoniemi, T. K. Yeoman, P. L. Dyson, R. A. Greenwald, T. Kikuchi, M. Pinnock, J. P. S. Rash, N. Sato, G. J. Sofko, J. P. Villain, and A. D. M. Walker (2007), A decade of the Super Dual Auroral Radar Network (SuperDARN): scientific achievements, new techniques and future directions, *Surv. Geophys.*, 28, 33-109.
7. Davies, K. (1990), Ionospheric Radio, The Institution of Engineering and Technology, London, U. K.
8. Eltrass, A., A. Mahmoudian, W. A. Scales, S. de Larquier, J. M. Ruohoniemi, J. B. H. Baker, R. A. Greenwald, and P. J. Erickson (2014), Investigation of the temperature gradient instability as the source of mid-latitude quiet-time decameter-scale ionospheric irregularities: Part 2, Linear analysis, *J. Geophys. Res.*, 119, doi:10.1002/2013JA019644.
9. Eltrass, A., and W. A. Scales (2014), Nonlinear evolution of the temperature gradient instability in the mid-latitude ionosphere, *J. Geophys. Res.*, 119, 1-13, doi:10.1002/2014JA020314.
10. Fejer, B. G., and M. C. Kelley (1980), Ionospheric irregularities, *Rev. Geophys.*, 18(2), 401-454, doi:10.1029/RG018i002p00401.
11. Foster, J. C., and F. J. Rich (1998), Prompt mid-latitude electric field effects during severe magnetic storms, *J. Geophys. Res.*, 103, 26367-26372.
12. Gary, S. P., and T. E. Cole (1983), Pedersen density drift instabilities, *J. Geophys. Res.*, Vol. 88, No. A12, pp.10, 104-10, 110.
13. Greenwald, R. A., K. Oksavik, P. J. Erickson, F. D. Lind, J. M. Ruohoniemi, J. B. H. Baker, and J. W. Gjerloev (2006), Identification of the temperature gradient instability as the source of decameter-scale ionospheric irregularities on plasmapause field lines, *Geophys. Res. Lett.*, VOL. 33, L18105, 419.
14. Hudson, M. K., and M. C. Kelley (1976), The temperature gradient instability at the equatorward edge of the ionospheric plasma trough, *J. Geophys. Res.*, 81, 3913- 3918.
15. Kelley, M. C. (2009), The Earth's ionosphere, plasma physics and electrodynamics, International Geophysics Series, 2nd ed., Elsevier.
16. Keskinen, M. J. (1984), Nonlinear theory of the E×B instability with an inhomogeneous electric field, *J. Geophys. Res.*, 89, 3913-3920.
17. Keskinen, M. J., and J. D. Huba (1990), Nonlinear evolution of high-latitude ionospheric interchange instabilities with scale-size-dependent magnetospheric coupling, *Geophys. Res. Lett.*, 95, A9, 15157-15166.
18. Keskinen, M. J., S. Basu, and S. Basu (2004), Mid-latitude sub-auroral ionospheric small scale structure during a magnetic storm, *Geophys. Res. Lett.*, 31, L09811, doi:10.1029/2003GL019368.
19. Ledvina, B. M., J. J. Makela, and P. M. Kintner (2002), First observations of intense GPS L1 amplitude scintillations at midlatitude, *Geophys. Res. Lett.*, 29(14), 1659, doi:10.1029/2002GL014770.
20. Mishin, E. V., W. J. Burke, C. Y. Huang, and F. J. Rich (2003), Electromagnetic wave structures within sub-auroral polarization streams, *J. Geophys. Res.*, 108(A8), 1309, doi:10.1029/2002JA009793.
21. Mishin, E. V., and N. Blaunstein (2008), Irregularities within sub-auroral polarization stream-related troughs and GPS radio interference at mid-latitudes, *AGU Geophysical Monograph 181*, Mid-Latitude Ionospheric Dynamics and Disturbances, pp. 291-295, doi:10.1029/181GM26, Washington, DC, USA.
22. Oksman, J., H. G. Moller, and R. Greenwald (1979), Comparisons between strong HF backscatter and VHF radar aurora, *Radio Sci.*, 14(6), 1121-1133.
23. Singleton, D. G. (1974), Power spectra of ionospheric scintillations, *J. Atmos. Terr. Phys.*, 36, 113-133.
24. Van Dierendonck, A. J., J. Klobuchar, and Q. Hua (1993), Ionospheric scintillation monitoring using commercial single frequency c/a code receivers, in Proceedings of the 6th International Technical Meeting of the Satellite Division of The Institute of Navigation (ION GPS 1993), pp. 1333-1342, Salt Lake City, UT, September 1993.